


 Cite this: *Chem. Commun.*, 2022, 58, 6689

 Received 11th April 2022,  
 Accepted 13th May 2022

DOI: 10.1039/d2cc02021a

[rsc.li/chemcomm](https://rsc.li/chemcomm)

# Novel thiophene-based donor–acceptor scaffolds as cathodes for rechargeable aqueous zinc-ion hybrid supercapacitors†

 Haijun Peng,<sup>a</sup> Yongxiang Zheng,<sup>b</sup> Cyril Antheaume,<sup>a</sup> Paolo Samori \*<sup>a</sup> and Artur Ciesielski \*<sup>a</sup>

Well-defined  $\pi$ -conjugated thiophene donor–acceptor molecules play an important role in different fields ranging from synthetic chemistry to materials science. Their chemical structure provides specific electronic and physicochemical properties, which can be further tuned by the introduction of functional groups. Herein, we design and synthesize two novel thiophene-based  $\pi$ -conjugated donor–acceptor molecules TDA-1 and TDA-2 through Aldol and Knoevenagel condensations. In our proof-of-concept study we report for the first time on the use of small organic molecules employed in aqueous zinc-ion hybrid supercapacitors (Zn-HSCs), which exhibit capacitance as high as 206.7 and 235.2 F g<sup>-1</sup> for TDA-1, and TDA-2, respectively.

The need to power portable and wearable electronic devices calls for the development of novel, high-performance and sustainable energy storage systems (ESS) and technologies.<sup>1–3</sup> The limited and uneven distribution of lithium reserves across the globe sparks the emergence of new energy storage solutions relying on other metal cations, including sodium (Na<sup>+</sup>), potassium (K<sup>+</sup>), magnesium (Mg<sup>+</sup>), aluminum (Al<sup>3+</sup>), and zinc (Zn<sup>2+</sup>), *etc.*<sup>4–7</sup> Among them, zinc-ions are particularly suitable as an anode material in supercapacitors because of their high theoretical capacity (823 mA h g<sup>-1</sup>, Zn/Zn<sup>2+</sup>). Furthermore, the use of Zn electrodes allows lowering the electrochemical potential by 0.76 V when compared to standard hydrogen electrodes. Endeavour in this direction led to the development of zinc-ion hybrid supercapacitors (Zn-HSCs) which are emerging energy storage systems holding the potential to meet industrial requirements due to their inherent safety features, low cost of

production, and natural abundance of Zn, as compared to lithium.<sup>8–12</sup>

Small organic molecules such as quinones,<sup>13</sup> imines,<sup>14</sup> ketones,<sup>15</sup> and aza derivatives<sup>16</sup> are extensively explored as electrode active materials in energy storage applications because of their low molecular weights, wide structural and functional diversity, and chemical tunability.<sup>17,18</sup> Small organic molecules, compared to polymers typically employed in Zn-HSCs, provide more active sites, *i.e.*, moieties capable to interact with metal ions through non-covalent (typically coordination) bonds per unit volume, which is beneficial for improving the areal capacitance. Among them, molecules comprising redox-active moieties, acting as charge-storage centers, surrounded by redox-inert organic groups operating as an insulating barrier, have been widely explored in various supercapacitor architectures,<sup>19,20</sup> and received significant interest in zinc-ion batteries due to their structural tunability and redox properties that can be encoded by molecular design.

As redox-active molecules, various organic quinone-based compounds have been designed for application as active electrode materials in Zn<sup>2+</sup> energy storage devices. For example, Chen *et al.* reported on a remarkable performance of calix[4]quinone electrodes in zinc-ion batteries, which display an energy density as high as 220 W h kg<sup>-1</sup>.<sup>21</sup> Xia *et al.* constructed an environmentally friendly and flexible aqueous zinc battery based on a pyrene-4,5,9,10-tetraone derivative, which exhibits a high energy density of 186.7 W h kg<sup>-1</sup> and long-term lifespan over 1000 cycles.<sup>22</sup> More recently, Markus *et al.* and Sun *et al.* demonstrated that small tetrachloro-*p*-benzoquinone and tetraamino-*p*-benzoquinone molecules can be successfully used as cathodes yielding 213 mA h g<sup>-1</sup> capacity under current density of 5 A g<sup>-1</sup> for 1000 in aqueous zinc-organic batteries.<sup>23,24</sup> However the organic molecules exploited so far for aqueous zinc-ion based ESS such as batteries and supercapacitors generally deliver low specific capacity/capacitance due to the limited amount of available active sites capable of interacting with Zn<sup>2+</sup> ions during device operation (*viz.* charge/discharge), which might be associated with poor

<sup>a</sup> University of Strasbourg CNRS, ISIS UMR 7006, 8 Allée Gaspard Monge, Strasbourg F-67000, France. E-mail: samori@unistra.fr, ciesielski@unistra.fr

<sup>b</sup> University of Strasbourg Membrane Biophysics and NMR, Institute of Chemistry, UMR 7177, 1 Rue Blaise Pascal, Strasbourg F-67000, France

† Electronic supplementary information (ESI) available. See DOI: <https://doi.org/10.1039/d2cc02021a>



molecular design, *i.e.*, the lack of the coordination sites in the molecular structures. On the other hand, the use of molecules bearing moieties that could form strong coordination bonds, such as carbonyls, might result in propensity to generate too strong non-covalent bonds with zinc ions in the operating device, limiting  $\text{Zn}^{2+}$  release during the discharge. Hence, the design of novel molecules embedding many active sites which can interact through weak thus reversible supramolecular bonds with the ions holds great potential for the development of high-performance EES.

Compared with redox-active (macro)molecules, donor-acceptor (DA) dyads and multiads are still underexplored for applications as electrode materials for energy storage application,<sup>25–27</sup> yet, they appear more appealing as the redox properties of the donor and acceptor moieties can be individually tuned through chemical design and integrated into SCs devices.<sup>28</sup> In particular, the possibility of having a two-component system such as DA, where the intramolecular charge transfer between the donor and acceptor can significantly increase the operating voltage (depending on the applied potential), can improve the electron transfer between electrode and electrolyte, ultimately boosting the performance of Zn-HSC.

Herein, we report on the synthesis of two novel thiophene-based small  $\pi$ -conjugated donor-acceptor molecules, *i.e.*, **TDA-1** and **-2**. The unique design of **TDA-1** comprises electron rich thiophenes whose unpaired electrons can serve as  $\text{Zn}^{2+}$  storage site and through the formation of discrete supramolecular assemblies can potentially generate percolation pathways for the diffusion of ions. On the other hand, the electron deficient triazine in **TDA-1** and cyano units in **TDA-2** are expected to promote intramolecular charge transfer facilitating the charge transfer between the electrode and electrolyte. Micrometer thick hybrid films comprising **TDA-1** or **TDA-2** and conductive porous carbon (Super P) were exploited as cathodes in a two-electrode coin cell of aqueous Zn-HSCs (see details in the ESI†). The latter devices exhibit high capacitance of 206.7 and 235.2  $\text{F g}^{-1}$ , respectively, and good reversible capacity of  $\approx 112.5$  and 98.6  $\text{F g}^{-1}$  when **TDA-1** and **TDA-2** was used, respectively, after 400 cycles at a current density of 1  $\text{A g}^{-1}$ .

This study demonstrates how the rational design of novel  $\pi$ -conjugated donor-acceptor molecules can be key for their use as cathodes in of aqueous Zn-HSC displaying high-performance. The synthesis of the thiophene-based donor-acceptor **TDA-1** and **TDA-2** scaffolds was accomplished by means of Aldol and Knoevenagel condensations (Fig. 1), in which the thiophene-2-carbaldehyde acted as donor unit, and 2,4,6-trimethyl-1,3,5-triazine and 1,3,5-benzenetriacetonitrile were employed as acceptor units (the details can be found in the ESI†).

All compounds were characterized by nuclear magnetic resonance (NMR) with the assistance of ultra-high-performance liquid chromatography high-resolution mass spectrometer (Fig. S9, ESI†). 2D-heteronuclear and 1D-NMR analyses were performed to elucidate the molecular structure of **TDA-1** and **TDA-2** molecules by assigning all the  $^1\text{H}$  (500 MHz) and  $^{13}\text{C}$  (125 MHz) signals. The chemical structures

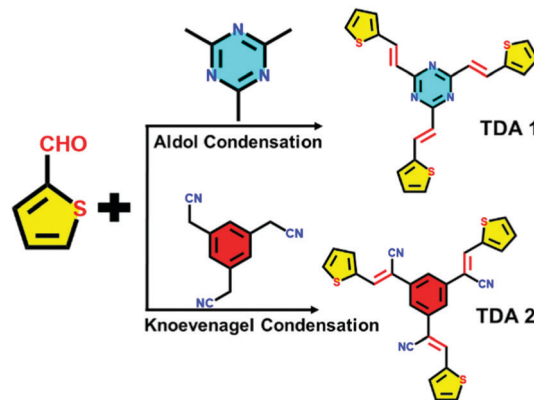


Fig. 1 Schematic illustration of the synthetic route of **TDA-1** and **-2** molecules.

of **TDA-1** and **TDA-2** were confirmed by 2D NMR through heteronuclear single quantum coherence (HSQC) and heteronuclear multiple bond correlation (HMBC) spectroscopy. Both  $^1\text{H}$ - $^{13}\text{C}$  HSQC and  $^1\text{H}$ - $^{13}\text{C}$  HMBC experiments were shown to be very powerful to correlate each proton with its corresponding carbon and link the different spin systems to assign the quaternary carbons.<sup>29</sup>

In particular, the proton spectra show an AX spin-system with a strong coupling constant of 15.5 Hz specific to an *E*-isomer of a double bond for H-3 and H-4. The chemical shift of olefin carbon C-4 at 134.6 ppm in **TDA-1** was confirmed through correlation H-4 protons at 8.36 ppm in the HSQC spectra and the multi-band coupling with thiophene-units C-6 at 130.6 ppm in the HMBC spectra (Fig. 2(a)). The pseudo triplet H-7 at 7.08 ppm is in-between H-8 and H-6 of the ABX thiophene unit. Based on 1D and 2D-NMR findings (Fig. S1–S4, ESI†), all  $^1\text{H}$  and  $^{13}\text{C}$  NMR signals of **TDA-1** could be unambiguously assigned (Table S1, ESI†).

Upon using the same carbon skeleton numbering for **TDA-2**, the chemical shift of olefin carbon C-4 at 136.5 ppm was also confirmed by correlation with H-4 protons that appear now as a singlet at 7.81 ppm and the long-range coupling from one side with the thiophene-units carbons Cq-5 at 137.5 ppm (Fig. 2(b)), CH-6 at 133.9, and from the other side with Cq-3,3' respectively at 136.0 and 117.8 ppm. The benzene protons singlet H-1 at 7.83 ppm in the HMBC spectra gives long-range coupling with Cq-2 at 106.3 ppm and Cq-3. As in the case of **TDA-1**, the pseudo triplet H-7 of thiophene moiety gives a long-range coupling with Cq-5 at 137.4 ppm. A complete assignment of  $^1\text{H}$  and  $^{13}\text{C}$  NMR resonance spectra of **TDA-2** was therefore obtained (Fig. S5–S8 and Table S1, ESI†). Fourier transform infrared (FTIR) spectroscopy, UV/Vis spectroscopy and cyclic voltammetry are shown in Fig. S10–S14 (ESI†).

To evaluate the potential of **TDA-1** and **TDA-2** as cathodes in Zn-HSCs, we constructed aqueous Zn-HSC devices as illustrated in Fig. 3(a) with 2  $\text{mol L}^{-1}$   $\text{Zn}(\text{CF}_3\text{SO}_3)_2$  solution in a full coin cell. **TDA-1** and **TDA-2** are pasted onto a porous stainless steel current collector (Fig. 3(b)) which promotes the contact between active materials and electrolyte.



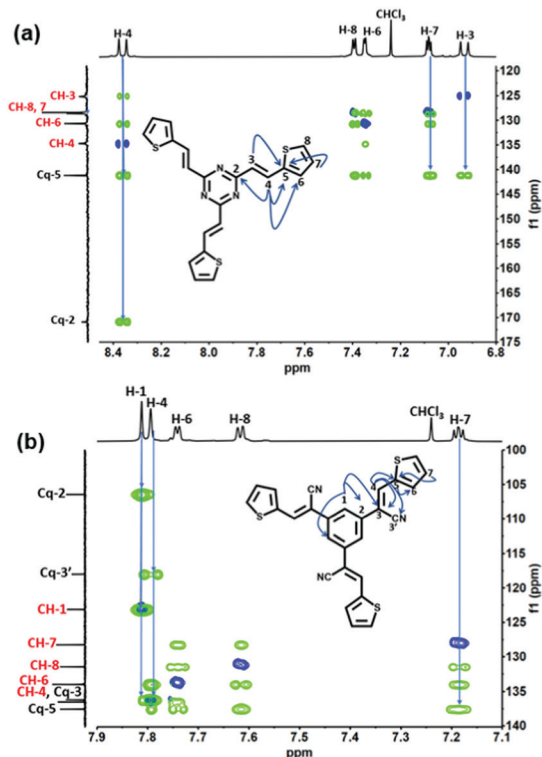


Fig. 2 (a)  $^1\text{H}$ - $^{13}\text{C}$  HSQC (blue) and key HMBC (green) of **TDA-1**. (b)  $^1\text{H}$ - $^{13}\text{C}$  HSQC (blue) and key HMBC (green) of **TDA-2**.

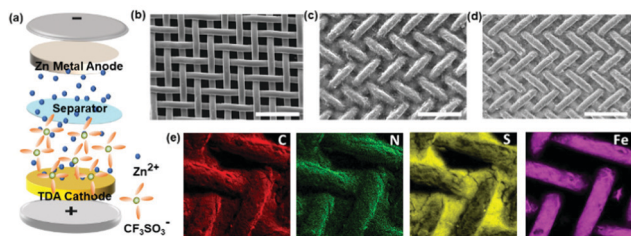


Fig. 3 (a) Schematic model of Zn-HSC energy storage system. (b) SEM image of pure stainless steel electrode. (c) SEM image of **TDA-1** on stainless steel electrode. (d) SEM image of **TDA-2** on stainless steel electrode. (e) Element mapping spectra of C, N, S, Fe on **TDA-1** electrode. Scale bars of (b–d) correspond to 200  $\mu\text{m}$ .

The **TDA-1** and **TDA-2** based electrodes were characterized by scanning electron microscopy (SEM) and energy-dispersive spectrometry (EDS). The SEM images of **TDA-1** (Fig. 3(c) and Fig. S15, ESI $^\dagger$ ) and **TDA-2** electrodes (Fig. 3(d) and Fig. S16, ESI $^\dagger$ ) revealed that **TDA-1** and **TDA-2** form aggregates of particles, which are distributed uniformly on the stainless-steel current collector. The corresponding EDS mapping of **TDA-1** (Fig. 3(e)) and **TDA-2** electrodes (Fig. S17, ESI $^\dagger$ ) further verified the presence of C, N, S elements with homogeneous elemental distribution on the stainless-steel current collector (Fe).

Subsequently, the  $\text{Zn}^{2+}$ -ion storage behavior of the **TDA-1** and **TDA-2** based electrodes was firstly evaluated by cyclic voltammetry (CV) experiments. The CV curves of the **TDA-1**



Fig. 4 Cyclic voltammetry curve of (a) **TDA-1**. (b) **TDA-2**. (c) The specific capacitance of **TDA-1** and **TDA-2** electrodes at different scan rates. (d)  $b$ -value in eqn (1) at two pairs redox peaks.

and **TDA-2** electrodes are shown in Fig. 4(a) and (b), respectively. Owing to the electrochemical adsorption and desorption of Zn ions on the thiophene-units in **TDA-1** and **TDA-2** during the CV process, a pair of strong redox peaks can be observed in the potential range of 0 to 1.6 V at different scan rates ranging between 10–200  $\text{mV s}^{-1}$ , which suggests that the presence of **TDA-1** and **TDA-2** molecules imparts pseudocapacitance to the devices. The shape of the voltammograms curve was well maintained even at a high scan rate of 200  $\text{mV s}^{-1}$ , indicating excellent charge transfer kinetics at the surface of the **TDA-1** and **TDA-2** electrodes.<sup>28,30</sup> For comparison, a pure Super-P carbon black electrode was also constructed and tested as a Zn-HSC cathode. The CV voltammograms of the neat Super-P did not reveal a presence of any redox peaks between different voltage range (Fig. S18, ESI $^\dagger$ ). **TDA-1** and **-2** based Zn-HSC devices showed a typical pseudocapacitive behavior, which may originate from the presence of active groups in the **TDA-1** and **TDA-2** moieties.

The specific capacitance values of **TDA-1** and **TDA-2** based Zn-HSC calculated from the CV curves acquired at 10, 20, 50, 100, and 200  $\text{mV s}^{-1}$  amount to 206.7, 181.4, 163.4, 156.2, and 113.7  $\text{F g}^{-1}$  for **TDA-1**, and 235.2, 206.6, 191.3, 184.2 and 139.7  $\text{F g}^{-1}$  for **TDA-2**, respectively (Fig. 4(c)).

To further investigate the  $\text{Zn}^{2+}$  storage properties, galvanostatic charge/discharge (GCD) curves were recorded and are shown in Fig. S19 and S20 (ESI $^\dagger$ ). The distorted triangular shape of the GCD curves revealed the pseudocapacitive behavior of **TDA-1** and **TDA-2**, which is consistent with the CV analysis. The  $\text{Zn}^{2+}$  storage kinetics of **TDA-1** and **TDA-2** electrodes were studied by the method proposed by Dunn *et al.*<sup>31</sup> The relationship of the peak current  $I$  and scan rate  $\nu$  from CV follows the equation of  $I = a\nu^b$ , where the  $b$  value of 0.5 is indicative of a diffusion-controlled process and a  $b$  value of 1.0 identifies a capacitor-controlled process. Fig. 4(d) displays the dependence between  $\log(I)$  versus  $\log(\nu)$  for oxidation (O) and



reduction (R) peaks O1, R1, O2, and R2. The fitting slopes for O1, R1, O2, and R2 are 0.85, 0.81, 0.78, and 0.83 respectively. These high *b*-values suggest the domination of the capacitor-controlled process and indicate facile reaction kinetics of **TDA-1** and **TDA-2** electrodes. Electrochemical impedance spectroscopy measurement was further performed to evaluate the diffusion resistance of **TDA-1** and **-2** based electrodes. As shown in Fig. S21 (ESI<sup>†</sup>), the Nyquist plot indicated an obvious supercapacitor behavior and lower charge transfer resistance and ionic diffusion resistance between **TDA-1** and **TDA-2** based electrode and the aqueous electrolyte.<sup>32</sup> Moreover, the long-term cycling test of **TDA-1** and **TDA-2** based electrodes at 1 A g<sup>-1</sup> exhibited a good reversible capacity of ≈112.5 and 98.6 F g<sup>-1</sup>, respectively, after 400 cycles (Fig. S22, ESI<sup>†</sup>), which is superior to the most of the recently reported inorganic and organic compounds cathode materials employed for aqueous Zn-HSCs (Table S2, ESI<sup>†</sup>). Noteworthy, the morphology of the **TDA-1** and **TDA-2** electrodes after 400 cyclic performance does not show any obvious change, which could indicate their high stability during charge-discharge process (Fig. S23, ESI<sup>†</sup>). These results suggest that the electron donor-acceptor of thiophene-units present in small organic molecules play a key role in increasing the electrochemical performance due to the intramolecular charge transfer, but the precise mechanism of the thiophene-units in Zn<sup>2+</sup> ion energy storage still needs further exploration, which is ongoing in our next project.

In summary, we have synthesized two novel thiophene-based donor-acceptor molecules by Aldol and Knoevenagel condensations. The presence of both donor and acceptor moieties in the structure of the molecules allows facilitated intramolecular charge transport and storage of Zn ions. The structures of the as-synthesized **TDA-1** and **TDA-2** were elucidated by means of 2D NMR of HSQC and HMBC spectroscopies. As a prototypical application, **TDA-1** and **TDA-2** based Zn-HSCs devices were fabricated. They exhibited a high specific capacitance of 206.7, and 235.2 F g<sup>-1</sup>, respectively. The superior performance may originate from the two pairs of lone electrons in doped thiophene moieties, which facilitate Zn<sup>2+</sup> transportation and charge transfer between the electrode and the electrolyte. This study provides unambiguous evidence on the importance of the rational design of  $\pi$ -conjugated donor-acceptor molecules to be used as cathodes in aqueous Zn-HSC displaying high-performance. Such small molecules represent novel scaffolds whose unique design renders them particularly interesting for applications in metal-ion capacitors, organic field-effect transistors, organic photovoltaics, and solar cells.

We acknowledge the financial support from the European Commission through the Marie Skłodowska-Curie project ULTIMATE (GA-813036), the Agence Nationale de la Recherche through the Labex project CSC (ANR-10-LABX-0026 CSC) within the Investissement d'Avenir program (ANR-10-120 IDEX-0002-02), the International Center for Frontier Research in Chemistry (icFRC), the Institut Universitaire de France (IUF) and the Chinese Scholarship Council.

## Conflicts of interest

There are no conflicts to declare.

## Notes and references

- J. R. Miller and P. Simon, *Science*, 2008, **321**, 651–652.
- P. Simon and Y. Gogotsi, *Nat. Mater.*, 2008, **7**, 845–854.
- P. Zhang, F. Wang, M. Yu, X. Zhuang and X. Feng, *Chem. Soc. Rev.*, 2018, **47**, 7426–7451.
- N. Zhang, F. Cheng, Y. Liu, Q. Zhao, K. Lei, C. Chen, X. Liu and J. Chen, *J. Am. Chem. Soc.*, 2016, **138**, 12894–12901.
- Y. Fu, Q. Wei, G. Zhang, X. Wang, J. Zhang, Y. Hu, D. Wang, L. Zuin, T. Zhou, Y. Wu and S. Sun, *Adv. Energy Mater.*, 2018, **8**, 1801445.
- D. Chao, W. Zhou, C. Ye, Q. Zhang, Y. Chen, L. Gu, K. Davey and S.-Z. Qiao, *Angew. Chem., Int. Ed.*, 2019, **58**, 7823–7828.
- Z. Li, D. Chen, Y. An, C. Chen, L. Wu, Z. Chen, Y. Sun and X. Zhang, *Energy Stor. Mater.*, 2020, **28**, 307–314.
- Q. Liu, H. Zhang, J. Xie, X. Liu and X. Lu, *Carbon Energy*, 2020, **2**, 521–539.
- Z. Li, Y. An, S. Dong, C. Chen, L. Wu, Y. Sun and X. Zhang, *Energy Storage Mater.*, 2020, **31**, 252–266.
- X. Gong, J. Chen and P. S. Lee, *Batteries Supercaps*, 2021, **4**, 1529–1546.
- Y. Lu, Z. Li, Z. Bai, H. Mi, C. Ji, H. Pang, C. Yu and J. Qiu, *Nano Energy*, 2019, **66**, 104132.
- P. Ruan, S. Liang, B. Lu, H. J. Fan and J. Zhou, *Angew. Chem., Int. Ed.*, 2022, e202200598.
- W. Xiong, W. Huang, M. Zhang, P. Hu, H. Cui and Q. Zhang, *Chem. Mater.*, 2019, **31**, 8069–8075.
- M. Mao, C. Luo, T. P. Pollard, S. Hou, T. Gao, X. Fan, C. Cui, J. Yue, Y. Tong, G. Yang, T. Deng, M. Zhang, J. Ma, L. Suo, O. Borodin and C. Wang, *Angew. Chem., Int. Ed.*, 2019, **58**, 17820–17826.
- S. Wang, L. Wang, K. Zhang, Z. Zhu, Z. Tao and J. Chen, *Nano Lett.*, 2013, **13**, 4404–4409.
- L. Dong, Y. Chen, F. Zhai, L. Tang, W. Gao, J. Tang, Y. Feng and W. Feng, *J. Mater. Chem. A*, 2020, **8**, 18668–18676.
- X. Zeng, J. Hao, Z. Wang, J. Mao and Z. Guo, *Energy Storage Mater.*, 2019, **20**, 410–437.
- X. Yin, S. Sarkar, S. Shi, Q.-A. Huang, H. Zhao, L. Yan, Y. Zhao and J. Zhang, *Adv. Funct. Mater.*, 2020, **30**, 1908445.
- Q. Li, M. Horn, Y. Wang, J. MacLeod, N. Motta and J. Liu, *Materials*, 2019, **12**, 703.
- Y. Xu, X. Chen, C. Huang, Y. Zhou, B. Fan, Y. Li, A. Hu, Q. Tang and K. Huang, *J. Power Sources*, 2021, **488**, 229426.
- Q. Zhao, W. Huang, Z. Luo, L. Liu, Y. Lu, Y. Li, L. Li, J. Hu, H. Ma and J. Chen, *Sci. Adv.*, 2018, **4**, ea01761.
- Z. Guo, Y. Ma, X. Dong, J. Huang, Y. Wang and Y. Xia, *Angew. Chem., Int. Ed.*, 2018, **57**, 11737–11741.
- Z. Lin, H.-Y. Shi, L. Lin, X. Yang, W. Wu and X. Sun, *Nat. Commun.*, 2021, **12**, 4424.
- D. Kundu, P. Oberholzer, C. Glaros, A. Bouzid, E. Tervoort, A. Pasquarello and M. Niederberger, *Chem. Mater.*, 2018, **30**, 3874–3881.
- J.-S. Wu, S.-W. Cheng, Y.-J. Cheng and C.-S. Hsu, *Chem. Soc. Rev.*, 2015, **44**, 1113–1154.
- H. Jiang, J. Jin, Z. Wang, W. Wang, R. Chen, Y. Tao, Q. Xue, C. Zheng, G. Xie and W. Huang, *Research*, 2021, **2021**, 9525802.
- A. Benito-Hernández, M. T. El-Sayed, J. T. López Navarrete, M. C. Ruiz Delgado and B. Gómez-Lor, *Org. Chem. Front.*, 2018, **5**, 1748–1755.
- T. Li, X. Yan, W.-D. Zhang, W.-K. Han, Y. Liu, Y. Li, H. Zhu, Z. Li and Z.-G. Gu, *Chem. Commun.*, 2020, **56**, 14187–14190.
- P. Giraudeau, Y. Shrot and L. Frydman, *J. Am. Chem. Soc.*, 2009, **131**, 13902–13903.
- F. Zhao, Y. Wang, X. Xu, Y. Liu, R. Song, G. Lu and Y. Li, *ACS Appl. Mater. Interfaces*, 2014, **6**, 11007–11012.
- H.-S. Kim, J. B. Cook, H. Lin, J. S. Ko, S. H. Tolbert, V. Ozolins and B. Dunn, *Nat. Mater.*, 2017, **16**, 454–460.
- Z. Yang, J. Liu, Y. Li, G. Zhang, G. Xing and L. Chen, *Angew. Chem., Int. Ed.*, 2021, **60**, 20754–20759.

